01

Recombination of charge carriers in $CsPbBr_3$ films with high quantum photoluminescence efficiency

© A.S. Polushkin,[1] S.V. Makarov[1,2]

[1] ITMO University,
197101 St. Petersburg, Russia
[2] Qingdao Innovation and Development Center, Harbin Engineering University,
266000 Qingdao, Shandong, China
e-mail: s.makarov@metalab.ifmo.ru

Received May 22, 2024
Revised July 15, 2024
Accepted July 16, 2024

This work examines perovskite thin films produced by two different methods: the scalable slot-die coating method and the classical spin-coating method. To model the recombination of charge carriers in these films, the proven ABC model was used, which allows us to calculate recombination constants based on photoluminescence decay and the photoluminescence quantum yield. In addition, data were analyzed at different pump powers, which made it possible to obtain recombination constants with higher accuracy.

Keywords: halide perovskite, slot-die coating, luminescence decay, ABC- model.

DOI: 10.61011/TP.2024.10.59353.189-24

Introduction

Lead halide perovskites constitute a class of semiconductor materials with very attractive properties for optoelectronics [1,2]. They provide an opportunity to examine various phenomena in structures based on them [3–6] and, consequently, attract considerable research interest. The high photoluminescence quantum yield and its resistance to perovskite defects enable the use of printing methods for fabrication of thin-film light-emitting devices based on them [7–8]. Their high refraction index and well-pronounced exciton resonance at room temperature make perovskites promising materials for photonic structures and lasers [11–14]. In addition, perovskites are used to fabricate solar cells [15–17], photodetectors [18–19], transistors [20], and gas sensors [21–23].

A wide variety of perovskite-based light-emitting devices have been demonstrated since 2014 [24–27]. In addition, perovskite materials may be used in display production indirectly (as luminance and backlight enhancers) [28]. However, most of the tested perovskite devices were fabricated and operate only in laboratory conditions, and much additional research on optimizing the long-term stability and scaling-up of perovskite LEDs is needed to ready them for commercial use [29]. Thus, the development of scalable methods for deposition of perovskite thin films is an essential step toward commercialization of perovskite light-emitting devices [30,31].

A method for fabrication of perovskite-based light-emitting electrochemical cells by slot-die coating with hot air drying has recently been presented in [32]. The morphology and optical properties of composite films with perovskite nanocrystals prepared by various methods were investigated in this study. The quantum yield of photoluminescence and its decay were measured for $CsPbBr_3$ perovskite films with polyethylene oxide. Although the kinetics of photoluminescence in perovskites of this composition has recently investigated in [33], no in-depth studies of carrier recombination in films with larger grains fabricated using a scalable method have been performed yet.

The present study is focused on developing a model that characterizes the process of carrier recombination in $CsPbBr_3$ films fabricated by slot-die coating. The primary objective was to determine the coefficients of radiative and non-radiative recombination based on the kinetics of photoluminescence decay. These coefficients allow one to calculate the photoluminescence quantum yield and compare it with experimental data obtained earlier. The modeling results should be of value for researchers working on perovskite LEDs and in related fields where the quality of the $CsPbBr_3$ perovskite is of key importance.

1. Results

Four types of films made of $CsPbBr_3$ perovskite with polyethylene oxide have been examined experimentally in our previous study [32]. The films were produced using different printing methods. Two of them were fabricated by spin-coating with and without hot air drying and annealed at a temperature of 200°C. The other two films were produced by slot-die coating with or without simultaneous air drying and were also annealed afterwards. The morphology of films and their optical properties were studied. Time dependences of photoluminescence decay and dependences of the photoluminescence quantum yield on the pump power were obtained for all films (Fig. 1). However, carrier recombination in these films has not been

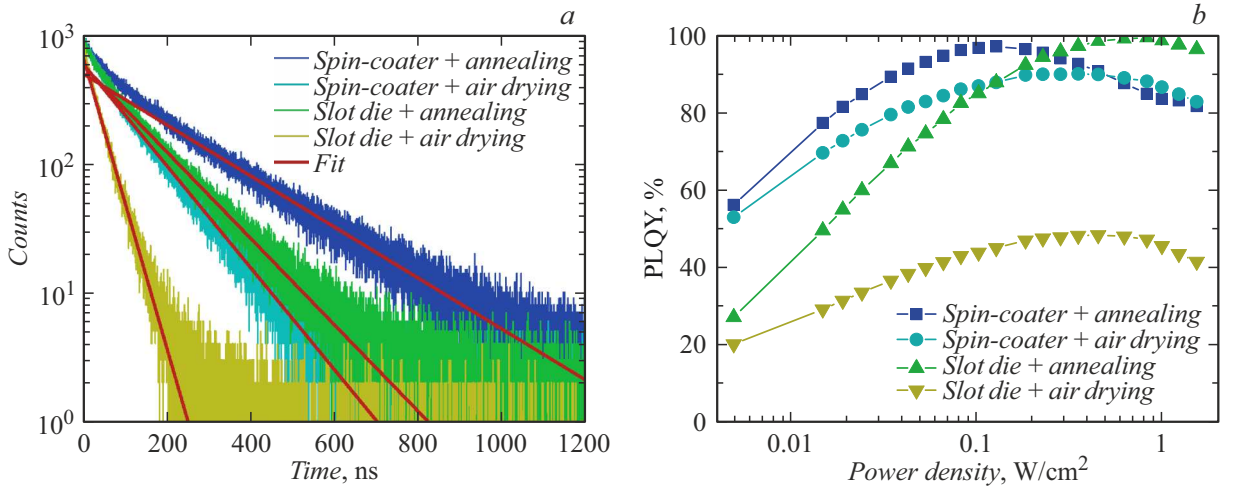

Figure 1. *a* — Experimental [32] photoluminescence decay of $CsPbBr_3$ films fabricated by different methods under pumping at $0.1\,\mu J/cm^2$ (noisy lines) and photoluminescence decay determined in the present study using approximation (3) (red straight lines); *b* — dependence of the photoluminescence quantum yield of $CsPbBr_3$ films synthesized by different methods on the pump power [32].

discussed in detail. A theoretical model characterizing the carrier kinetics in a perovskite film based on time-resolved photoluminescence spectroscopy could be used to estimate the photoluminescence quantum yield [34].

The simplified ABC model [35] may be used to characterize the recombination of charge carriers. Although this model is not necessarily suitable for all halide perovskites, it is still quite adequate at low carrier densities [36]. Let us examine a thin perovskite film on a glass substrate that is exposed to an ultrashort laser pulse. Electron–hole pairs are produced under the influence of photons; the density of holes is the same as the density of electrons, and there is no diffusion of carriers into the substrate. Electron density n may then be calculated using the following formula:

$$-\frac{dn}{dt} = An + Bn^2 + Cn^3. \qquad (1)$$

The first, second, and third terms here correspond to non-radiative recombination at defects (Shockley–Read–Hall recombination), radiative recombination, and Auger recombination, respectively. At low carrier densities (below $10^{18}\,cm^{-3}$), Auger recombination in perovskites may be neglected [37], since the third term is very small compared to the first two. Therefore, it is precisely these low densities (i.e., low pump powers) that will be considered. In fact, the model may be simplified further if the pump power is so low that the first term in Eq. (1) is much larger than the second: coefficient B is then also negligible, and Eq. (1) turns into a simple differential equation

$$\frac{dn}{dt} = -An. \qquad (2)$$

Solving it, we find

$$n(t) = n_0 \exp(-At) = n_0 \exp\left(-\frac{t}{\tau}\right), \qquad (3)$$

Table 1. Shockley–Read–Hall lifetime for $CsPbBr_3$ films

Sample	τ, ns
1	180
2	101
3	113
4	35

where n_0 is the electron density at $t = 0$ and $\tau = 1/A$ is the carrier lifetime at a low density (Shockley–Read–Hall time). Figure 1, *a* shows the photoluminescence decay curves of four perovskite films. Sample 1 is the film synthesized by spin-coating without hot air drying. Sample 2 was prepared by spin-coating with drying. Samples 3 and 4 were fabricated by slot-die coating without and with drying, respectively. Using formula (3), one may determine τ for all the samples from these curves. The red lines represent the results of approximation of photoluminescence decay by formula (3). The electron lifetimes determined this way are listed in Table 1.

Since the photoluminescence decay curve in Fig. 1, *a* is plotted on a logarithmic scale, an exponential decay in accordance with formula (3) should be represented by a straight line. The decay plot for sample 4 does indeed take the form of a straight line, but the approximation for sample 1 deviates from the experimental data in the vicinity of the initial time. This is attributable to bimolecular radiative recombination of electrons and holes, which implies that coefficient B for this sample cannot be neglected even at such a low power level. With an increase in pump power, the second term in Eq. (1) will also become non-negligible for the remaining samples. Thus, one needs to

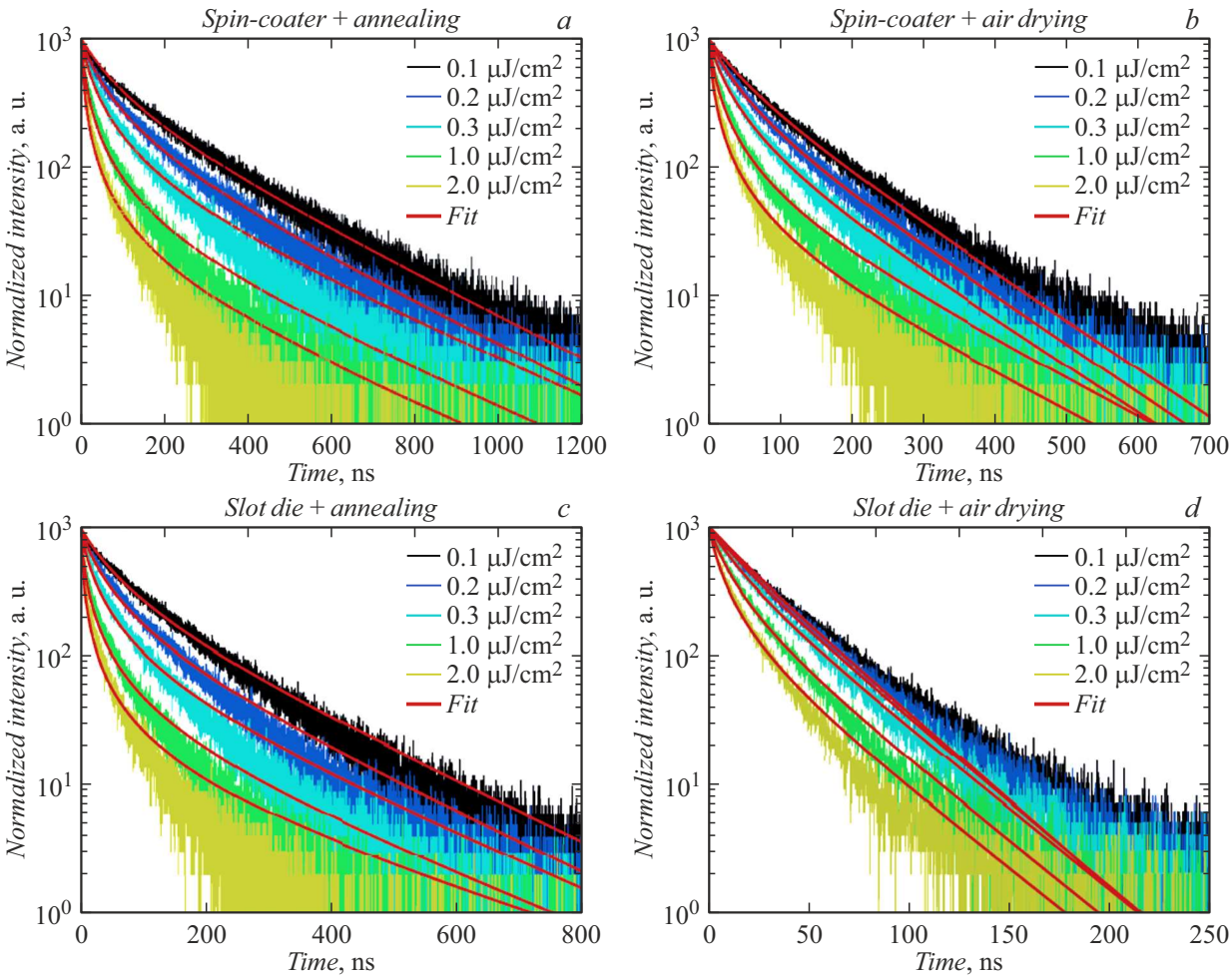

Figure 2. Experimental [32] photoluminescence decay and its approximation by formula (5) at different pump fluences for $CsPbBr_3$ films synthesized: *a* — by spin-coating without drying, *b* — by spin-coating with drying, *c* — by slot-die coating without drying, and *d* — by slot-die coating with drying.

solve differential equation

$$-\frac{dn}{dt} = An + Bn^2. \tag{4}$$

Its solution may be written as

$$n(t) = \frac{An_0 \exp(-At)}{A + Bn_0\big(1 - \exp(-At)\big)}. \tag{5}$$

Here, $n_0 = n(0)$ is the electron density at the initial moment of time. If the thickness of films and the absorbance of perovskite are known, one may estimate n_0 in the following way:

$$n_0 = \frac{4\alpha P}{h\nu f \pi d^2 w}, \tag{6}$$

where α is the film absorbance, P is the pump laser power, $h\nu$ is the pump photon energy, f is the pulse repetition rate, $\pi d^2/4$ is the laser spot area (d is the spot diameter), and w is the film thickness.

Thus, Eq. (5) allows one to determine coefficients A and B numerically based on the results of time-resolved spectroscopy. Figure 2 presents the photoluminescence decay curves at different pump fluences for all four samples. Approximating the attenuation with formula (5), we find A and n_0B numerically at different pump powers. Coefficient A depends on the density of defects in the sample. As the pump power increases, more and more defects are filled with electrons and become unsuited for recombination; therefore, coefficient A decreases with increasing pump power. The results of numerical calculation of coefficients A are presented in Table 2. Since the obtained film samples differ in thickness, they also differ in carrier density at one and the same pump energy level. Coefficient B is related to the interband transition probability, which is determined by the material type and, consequently, does not depend on the sample and the pump power. The value of parameter B in this approximation was $9.82 \cdot 10^{-10}\,\mathrm{cm}^3/\mathrm{s}$, which is consistent with the one given in literature [38]. The value of the radiative recombination coefficient for $CsPbBr_3$ single crystals reported in [39] is two orders of magnitude higher, but it was obtained at cryogenic temperatures (15 K).

Table 2. Coefficients A determined using formula (5) for all $CsPbBr_3$ films and various pump levels

Sample	F, μJ/cm^2	n_0, cm^{-3}	A, s^{-1}
1	0.1	$9.37 \cdot 10^{15}$	$3.76 \cdot 10^6$
	0.2	$1.87 \cdot 10^{16}$	$3.73 \cdot 10^6$
	0.4	$3.75 \cdot 10^{16}$	$3.27 \cdot 10^6$
	1	$9.37 \cdot 10^{16}$	$3.27 \cdot 10^6$
	2	$1.87 \cdot 10^{17}$	$3.18 \cdot 10^6$
2	0.1	$9.86 \cdot 10^{15}$	$8.63 \cdot 10^6$
	0.2	$1.97 \cdot 10^{16}$	$8.63 \cdot 10^6$
	0.4	$3.94 \cdot 10^{16}$	$8.30 \cdot 10^6$
	1	$9.86 \cdot 10^{16}$	$6.78 \cdot 10^6$
	2	$1.97 \cdot 10^{17}$	$6.59 \cdot 10^6$
3	0.1	$1.51 \cdot 10^{16}$	$5.38 \cdot 10^6$
	0.2	$3.03 \cdot 10^{16}$	$5.38 \cdot 10^6$
	0.4	$6.05 \cdot 10^{16}$	$4.89 \cdot 10^6$
	1	$1.51 \cdot 10^{17}$	$4.55 \cdot 10^6$
	2	$3.03 \cdot 10^{17}$	$3.54 \cdot 10^6$
4	0.1	$8.01 \cdot 10^{15}$	$3.12 \cdot 10^7$
	0.2	$1.60 \cdot 10^{16}$	$3.01 \cdot 10^7$
	0.4	$3.20 \cdot 10^{16}$	$2.88 \cdot 10^7$
	1	$8.01 \cdot 10^{16}$	$2.88 \cdot 10^7$
	2	$1.60 \cdot 10^{17}$	$2.83 \cdot 10^7$

Coefficient A characterizes the process of recombination at defects. Its value may be used for qualitative assessment of the defects concentration in a sample: the higher coefficient A is, the higher is the defects concentration in a film. The lowest values of coefficient A were obtained for samples 1 and 3. This is consistent with the results of experimental measurements of the photoluminescence quantum yield: it was the highest for these samples (Fig. 1, *b*). Sample 4, on the contrary, has the highest coefficient A and, consequently, a higher concentration of defects. Therefore, its quantum yield is the lowest. A quantitative estimate of the defect concentration of the best samples (1 and 3) may be obtained in much the same way as it is done for $CH_3NH_3PbI_3$ perovskite films [40]. The defect concentration is then $3.05 \cdot 10^{15}$ and $3.40 \cdot 10^{15}$ cm^{-3} (at a pump level of 2 μJ/cm^2), respectively. These values match the defect concentrations determined earlier in $CsPbBr_3$ films and are an order of magnitude lower than the ones obtained in nanocrystals [39,41,42].

Having determined coefficients A and B from photoluminescence decay curves, one may estimate numerically the photoluminescence quantum yield (PLQY). Since PLQY is, by definition, the number of emitted photons divided by the total number of absorbed photons, the number of photons is related to the number of electrons at the initial time, and Auger recombination is lacking, we may express the yield as follows:

$$\mathrm{PLQY} = \frac{Bn^2}{An + Bn^2} = \frac{Bn_0}{A + Bn_0}. \qquad (7)$$

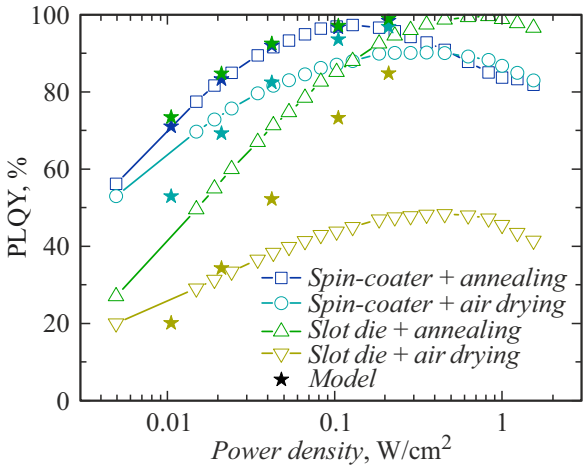

Figure 3. Experimental (symbols connected by lines [32]) and theoretically calculated (asterisks) dependences of the photoluminescence quantum yield for all four $CsPbBr_3$ films on the pump fluence.

Equation (7) allows one to calculate the photoluminescence quantum yield and compare it with the experimentally measured value. The PLQY measurement results are presented in Fig. 3. Open symbols represent the results of experimental PLQY measurement in an integrating sphere under irradiation by a continuous-wave laser diode with a wavelength of 405 nm. Asterisks correspond to the quantum yield values calculated theoretically by formula (7). It is evident that the experimental and theoretical values differ significantly. This discrepancy is attributable to the fact that the theoretical values were calculated based on the results of time-resolved spectroscopy performed with irradiation by a femtosecond laser with a pulse repetition rate of 100 kHz, while a continuous-wave laser was used in the experimental PLQY measurement. Under the influence of continuous radiation, defects in a material get filled with electrons and cease to be involved in recombination, which has a significant effect on the quantum yield. Under pulsed irradiation, electrons have enough time for relaxation, and the majority of defects are left unfilled and ready for recombination. For example, the number of defects is minimal for the sample obtained by spin-coating without drying. Therefore, the defect filling effect is largely irrelevant in this case, and the results of PLQY calculation agree closely with the experimentally measured values.

Conclusion

A model allowing one to calculate the coefficients of radiative (B) and non-radiative (A) recombination was developed based on the analysis of experimental data of time-resolved photoluminescence spectroscopy of $CsPbBr_3$ films. The values of these coefficients for perovskite films synthesized by slot-die coating have been determined for the first time. Coefficient B was found to be equal to

$9.82 \cdot 10^{-10}$ cm^3/s. The lowest values of the coefficient for recombination at defects $A = 3.18 \cdot 10^6$ and $3.54 \cdot 10^6$ s^{-1} (at a pump level of $2\,\mu$J/cm^2) were obtained in films synthesized by slot-die coating and spin-coating without hot air drying. These values correspond to a defect concentration of $3.05 \cdot 10^{15}$ and $3.40 \cdot 10^{15}$ cm^{-3}. A defect concentration this low is indicative of the high quality of perovskites of this type, which may be used in various optoelectronic film-based devices [40,41].

The resulting model estimates efficiently the concentration of defects in a sample and allows one to identify accurately the sample will the highest photoluminescence quantum yield. However, the results of calculation of the photoluminescence quantum yield based on the obtained recombination coefficients are not always consistent with the experimental data in the case of high defect concentrations. Nevertheless, the developed model may be used for rapid diagnostics of luminescent properties of high-quality perovskite films based on the results of photoluminescence decay measurements.

Funding

Time-resolved photoluminescence analysis was supported by a grant from the Russian Science Foundation (project 21-73-20189). The analysis of power dependences of photoluminescence quantum yield was supported by a grant from the Russian Science Foundation (project 24-79-10131).

Conflict of interest

The authors declare that they have no conflict of interest.

References

[1] P. Docampo, T. Bein. Accounts Chem. Research, **49**, 339 (2016).
[2] J. Liang, J. Liu, Z. Jin. Solar Rrl, **1**, 1700086 (2017).
[3] D.S. Gets, E.Y. Tiguntseva, A.S. Berestennikov, T.G. Lyashenko, A.P. Pushkarev, S.V. Makarov, A.A. Zakhidov. JETP Lett., **107**, 742 (2018).
[4] A.V. Andrianov, A.N. Aleshin, L. Matyushkin. JETP Lett., **109**, 28 (2019).
[5] K. Sekerbayev, Y.T. Taurbayev, I.N. Saraeva, S.I. Kudryashov, A.A. Ionin, V.Y. Timoshenko. JETP Lett., **110**, 592 (2019).
[6] K. Sekerbayev, G. Mussabek, N.S. Pokryshkin, V.G. Yakunin, Y.T. Taurbayev, Y. Shabdan, Z.N. Utegulov, V. Chirvony, V.Y. Timoshenko. JETP Lett., **114**, 447 (2021).
[7] Y. Wang, C. Duan, P. Lv, Z. Ku, J. Lu, F. Huang, Y.-B. Cheng. National Science Review, **8**, b075 (2021).
[8] J. Kang, L.-W. Wang. J. Phys. Chem. Lett., **8**, 489 (2017).
[9] X.-K. Liu, W. Xu, S. Bai, Y. Jin, J. Wang, R.H. Friend, F. Gao. Nature Mater., **20**, 10 (2021).
[10] D. Gets, D. Saranin, A. Ishteev, R. Haroldson, E. Danilovskiy, S. Makarov, A. Zakhidov. Appl. Surf. Sci., **476**, 486 (2019).
[11] S. Makarov, A. Furasova, E. Tiguntseva, A. Hemmetter, A. Berestennikov, A. Pushkarev, A. Zakhidov, Y. Kivshar. Adv. Opt. Mater., **7**, 1800784 (2019).
[12] Q. Zhang, Q. Shang, R. Su, T.T.H. Do, Q. Xiong. Nano Lett., **21**, 1903 (2021).
[13] I. Shishkin, A. Polushkin, E. Tiguntseva, A. Murzin, B. Stroganov, Y. Kapitonov, S.A. Kulinich, A. Kuchmizhak, S. Makarov. Appl. Phys. Express, **12**, 122001 (2019).
[14] A.O. Murzin, B.V. Stroganov, C. Gunnemann, S.B. Hammouda, A.V. Shurukhina, M.S. Lozhkin, A.V. Emeline, Y.V. Kapitonov. Adv. Opt. Mater., **8**, 2000690 (2020).
[15] J.Y. Kim, J.-W. Lee, H.S. Jung, H. Shin, N.-G. Park. Chem. Rev., **120**, 7867 (2020).
[16] D. Saranin, P. Gostischev, D. Tatarinov, I. Ermanova, V. Mazov, D. Muratov, A. Tameev, D. Kuznetsov, S. Didenko, A. Di Carlo. Materials, **12**, 1406 (2019).
[17] I. Turkevych, S. Kazaoui, N.A. Belich, A.Y. Grishko, S.A. Fateev, A.A. Petrov, T. Urano, S. Aramaki, S. Kosar, M. Kondo, E.A. Goodilin, M. Graetzel, A.B. Tarasov. Nature Nanotechnol., **14**, 57 (2019).
[18] W. Tian, H. Zhou, L. Li. Small, **13**, 1702107 (2017).
[19] F. Wang, X. Zou, M. Xu, H. Wang, H. Wang, H. Guo, J. Guo, P. Wang, M. Peng, Z. Wang, Y. Wang, J. Miao, F. Chen, J. Wang, X. Chen, A. Pan, Ch. Shan, L. Liao, W. Hu. Adv. Sci., **8**, 2100569 (2021).
[20] A.N. Aleshin, I.P. Shcherbakov, O.P. Chikalova-Luzina, L.B. Matyushkin, M.K. Ovezov, A.M. Ershova, I.N. Trapeznikova, V.N. Petrov. Synthetic Metals, **260**, 116291 (2020).
[21] A.A. Parfenov, O.R. Yamilova, L.G. Gutsev, D.K. Sagdullina, A.V. Novikov, B.R. Ramachandran, K.J. Stevenson, S.M. Aldoshin, P.A. Troshin. J. Mater. Chem. C, **9**, 2561 (2021).
[22] P.V. Shinde, A. Patra, C.S. Rout. J. Mater. Chem. C, **10**, 10196 (2022).
[23] D.I. Markina, S.S. Anoshkin, M.A. Masharin, S.A. Khubezhov, I. Tzibizov, D. Dolgintsev, I.N. Terterov, S.V. Makarov, A.P. Pushkarev. ACS Nano, **17**, 1570 (2023).
[24] Z.-K. Tan, R.S. Moghaddam, M.L. Lai, P. Docampo, R. Higler, F. Deschler, M. Price, A. Sadhanala, L.M. Pazos, D. Credgington, M. Kondo, F. Hanusch, Th. Bein, H.J. Snaith, R.H. Friend. Nature Nanotechnol., **9**, 687 (2014).
[25] A. Fakharuddin, M.K. Gangishetty, M. Abdi-Jalebi, S.-H. Chin, A.R. bin Mohd Yuso D.N. Congreve, W. Tress, F. Deschler, M. Vasilopoulou, H.J. Bolin. Nature Electron., **5**, 203 (2022).
[26] M. Alahbakhshi, A. Mishra, R. Haroldson, A. Ishteev, J. Moon, Q. Gu, J.D. Slinker, A.A. Zakhidov. ACS Energy Lett., **4**, 2922 (2019).
[27] D. Gets, M. Alahbakhshi, A. Mishra, R. Haroldson, A. Papadimitratos, A. Ishteev, D. Saranin, S. Anoshkin, A. Pushkarev, E. Danilovskiy, S. Makarov, J.D. Slinker, A.A. Zakhidov. Adv. Opt. Mater., **9**, 2001715 (2021).
[28] X.-G. Wu, H. Ji, X. Yan, H. Zhong. Nature Nanotechnol., **17**, 813 (2022).
[29] T.-H. Han, K.Y. Jang, Y. Dong, R.H. Friend, E.H. Sargent, T.-W. Lee. Nature Rev. Mater., **7**, 757 (2022).
[30] F.C. Krebs. Solar Energy Mater. Solar Cells, **93**, 394 (2009).
[31] T. Zhang, L. Wang, L. Kong, C. Zhang, H. He, B. Wei, X. Yang. J. Mater. Chem. C, **9**, 7532 (2021).
[32] A. Polushkin, E. Danilovskiy, E. Sapozhnikova, N. Kuzmenko, A. Pushkarev, S. Makarov. Photon. Nanostructures-Fundamentals and Applications, **58**, 101232 (2024).
[33] V. Baitova, M. Knyazeva, I. Mukanov, A. Tarasevich, A. Naumov, A. Son, S. Kozyukhin, I.Y. Eremchev. JETP Lett., **118**, 560 (2023).

[34] T. Kirchartz, J.A. Marquez, M. Stolterfoht, T. Unold. Adv. Energy Mater., **10**, 1904134 (2020).
[35] S. Karpov. Opt. Quant. Electron., **47**, 1293 (2015).
[36] A. Kiligaridis, P.A. Frantsuzov, A. Yangui, S. Seth, J. Li, Q. An, Y. Vaynzof, I.G. Scheblykin. Nature Commun., **12**, 3329 (2021).
[37] J.M. Richter, M. Abdi-Jalebi, A. Sadhanala, M. Tabachnyk, J.P. Rivett, L.M. Pazos-Outón, K.C. Gödel, M. Price, F. Deschler, R.H. Friend. Nature Commun., **7**, 13941 (2016).
[38] P. Ščajev, D. Litvinas, V. Soriutė, G. Kreiza, S. Stanionyte, S. Juršėnas. J. Phys. Chem. C, **123**, 23838 (2019).
[39] J. Peters, Z. Liu, R. Yu, K. McCall, Y. He, M. Kanatzidis, B. Wessels. Phys. Rev. B, **100**, 235305 (2019).
[40] P. Ščajev, S. Miasojedovas, S. Juršėnas. J. Mater. Chem. C, **8**, 10290 (2020).
[41] K. Abiedh, Z. Zaaboub, F. Hassen. Appl. Phys. A, **127**, 1 (2021).
[42] M. Zhang, Z. Zheng, Q. Fu, P. Guo, S. Zhang, C. Chen, H. Chen, M. Wang, W. Luo, Y. Tian. J. Phys. Chem. C, **122**, 10309 (2018).

Translated by D.Safin